Absence of Sac2/INPP5F enhances the phenotype of a Parkinson's disease mutation of synaptojanin 1

Mian Cao[a,b,c,d,1,2], Daehun Park[a,b,c,d,1], Yumei Wu[a,b,c,d], and Pietro De Camilli[a,b,c,d,e,3]

[a]Department of Neuroscience, Yale University School of Medicine, New Haven, CT 06510; [b]Department of Cell Biology, Yale University School of Medicine, New Haven, CT 06510; [c]Howard Hughes Medical Institute, Yale University School of Medicine, New Haven, CT 06510; [d]Program in Cellular Neuroscience, Neurodegeneration, and Repair, Yale University School of Medicine, New Haven, CT 06510; and [e]Kavli Institute for Neuroscience, Yale University School of Medicine, New Haven, CT 06510

Contributed by Pietro De Camilli, April 9, 2020 (sent for review March 9, 2020; reviewed by Volker Haucke and David Sulzer)

Numerous genes whose mutations cause, or increase the risk of, Parkinson's disease (PD) have been identified. An inactivating mutation (R258Q) in the Sac inositol phosphatase domain of synaptojanin 1 (SJ1/PARK20), a phosphoinositide phosphatase implicated in synaptic vesicle recycling, results in PD. The gene encoding Sac2/INPP5F, another Sac domain-containing protein, is located within a PD risk locus identified by genome-wide association studies. Knock-In mice carrying the SJ1 patient mutation (SJ1^{RQ}KI) exhibit PD features, while Sac2 knockout mice (Sac2KO) do not have obvious neurologic defects. We report a "synthetic" effect of the SJ1 mutation and the KO of Sac2 in mice. Most mice with both mutations died perinatally. The occasional survivors had stunted growth, died within 3 wk, and showed abnormalities of striatal dopaminergic nerve terminals at an earlier stage than SJ1^{RQ}KI mice. The abnormal accumulation of endocytic factors observed at synapses of cultured SJ1^{RQ}KI neurons was more severe in double-mutant neurons. Our results suggest that SJ1 and Sac2 have partially overlapping functions and are consistent with a potential role of Sac2 as a PD risk gene.

endocytosis | Sac2 | synaptojanin 1 | INPP5F | PI4P

Synaptojanin 1 (SJ1), also known as PARK20, is a phosphoinositide phosphatase concentrated at synapses implicated in endocytic membrane traffic. SJ1 dephosphorylates PI(4,5)P_2 on endocytic membranes via the sequential action of two tandemly arranged inositol phosphatase modules: a central 5-phosphatase domain and an N-terminal Sac phosphatase domain (Fig. 1*A*). The latter functions primarily as a 4-phosphatase domain, although it can also dephosphorylate PI3P and PI(3,5)P_2 in addition to PI4P in vitro (1).

Full loss-of-function mutations of the SJ1 gene result in early postnatal lethality in both mice and humans (2–4). In contrast, a homozygous missense R > Q mutation at amino acid position 258 within the Sac domain of SJ1 (a highly conserved amino acid position) is responsible for early-onset Parkinsonism (EOP) with epilepsy, leading to the naming of SJ1 as PARK20 (5–7).

The well-established main function of SJ1 is to participate in clathrin uncoating during the endocytic recycling of synaptic vesicles. SJ1 recruitment to endocytic pits by endophilin is required for dissociation of the PI(4,5)P_2-dependent interaction of the clathrin adaptors with the membrane (8–11). Such action cooperates in uncoating with the disassembly of the clathrin lattice mediated by the AAA ATPase HSC70 and its synaptically enriched cofactor auxilin (12, 13). Interestingly, loss-of-function mutations in auxilin (PARK19) also result in EOP with epilepsy (14–16). These observations support a link between dysfunction in clathrin-mediated budding and EOP.

We previously showed that the R258Q mutation abolishes the activity of the Sac phosphatase domain of SJ1 without affecting the activity of its 5-phosphatase domain (5). We also generated homozygous knock-in (KI) mice (SJ1^{RQ}KI mice) that carry the patient mutation and have neurologic manifestations reminiscent of those of human patients (17). Functional and microscopic analysis of cultured neurons and brain tissue of these mice demonstrated defects in synaptic vesicle recycling and dystrophic changes selectively in nerve terminals of dopaminergic neurons in the striatum (17). Levels of auxilin (PARK19) and other endocytic factors were abnormally increased in the brains of such mice (17). In addition, levels of the PD gene parkin (PARK2) were strikingly elevated (17), strengthening the evidence for a functional partnership among endophilin, SJ1, and parkin reported by previous studies (18–20).

Most interestingly, the intronic SNP rs117896735 located within the gene encoding Sac2/INPP5F, another protein conttaining a Sac domain that functions primarily as a PI4P 4-phosphatase (Fig. 1*A*) (21, 22), was identified as a risk locus in PD by genome-wide association studies (23, 24). Sac2 has been implicated in the endocytic pathway via its interaction with Rab5 and, like SJ1, is preferentially expressed in the nervous system (21, 22). These findings raise the hypothesis that the Sac domains of SJ1 and Sac2 may have some overlapping functions in the down-regulation of a same phosphoinositide pool on membranes of the endocytic pathway at synapses. Here we used mouse genetics to explore this possibility. We report the occurrence of a strong synthetic effect at both the organismal level and the synaptic level of the Sac2 null mutation and of the EOP mutation

Significance

Extensive genetic studies have identified numerous genes whose mutations results on Parkinson's disease (PD), including synaptojanin 1 (SJ1/Park20), a nerve terminal enriched protein that includes an inositol 4-phosphatase domain (Sac domain). In addition, many PD candidate genes have been identified by genome-wide association studies, but for most of these genes, the link to PD remains hypothetical. One such gene is Sac2/INPP5F, which, interestingly, also includes an inositol 4-phosphatase domain. While Sac2KO mice do not show obvious defects, we show a striking synthetic effect in mice of the KO of Sac2 and the Sac domain mutation of SJ1 found in PD patients. These findings support a synergistic role of SJ1 and Sac2 on a PI4P pool whose dysfunction results in PD.

Author contributions: M.C., D.P., Y.W., and P.D.C. designed research; M.C., D.P., and Y.W. performed research; M.C., D.P., Y.W., and P.D.C. analyzed data; and M.C., D.P., and P.D.C. wrote the paper.

Reviewers: V.H., Leibniz-Forschungsinstitut für Molekulare Pharmakologie and Freie Universität Berlin; and D.S., Columbia University.

The authors declare no competing interest.

[1]M.C. and D.P. contributed equally to this work.

[2]Present address: Program in Neuroscience and Behavioral Disorders, Duke-NUS Medical School, Singapore, 169857.

[3]To whom correspondence may be addressed. Email: pietro.decamilli@yale.edu.

This article contains supporting information online at https://www.pnas.org/lookup/suppl/doi:10.1073/pnas.2004335117/-/DCSupplemental.

First published May 18, 2020.

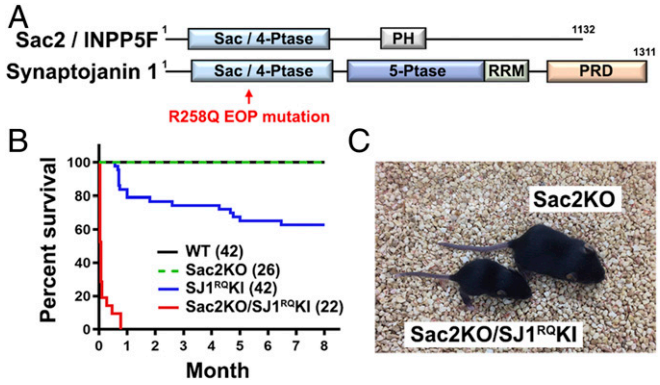

Fig. 1. Genetic interaction between SJ1 and Sac2/INPP5F. (*A*) Domain structures of SJ1 and Sac2. Sac/4-Ptase, 4-phosphatase domain; 5-Ptase, 5-phosphatase domain; RRM, RNA recognition motif; PRD, proline-rich domain; PH, pleckstrin homology. (*B*) Survival curves of mice with indicated genotypes. Numbers of animals are indicated in parentheses. (*C*) Littermate mice at P15. The Sac2KO/SJ1^{RQ}KI shown is one of the few survivors at this age.

in the Sac domain of SJ1. Our results support the identification of Sac2/INPP5F as the gene product responsible for the PD risk at SNP rs117896735 and corroborate evidence of a link between impaired endocytic flow at synapses and EOP.

Results

Synthetic Effect of SJ1 and Sac2 Mutations on Mice Survival. Sac2KO mice do not have an obvious pathological neurologic phenotype (25). Although SJ1^{RQ}KI mice are neurologically impaired and experience seizures, approximately 60% of them can reach adulthood (17). Mating of Sac2KO mice (26) to SJ1^{RQ}KI mice (17) to generate animals homozygous for both mutations revealed a striking genetic interaction between Sac2 and SJ1. Sac2KO/SJ1^{RQ}KI double-mutant mice were born with Mendelian ratio (*SI Appendix*, Fig. S1*A*) but had a dramatically shorter lifespan than SJ1^{RQ}KI mice (Fig. 1*B*). Most of them died within 24 h after birth, a few survived for a few days but failed to thrive, and the remainder died before weaning within 3 wk (Fig. 1 *B* and *C*). The Sac2 gene is adjacent to the Bag3 gene in both humans and mice, raising the possibility that a PD-relevant SNP found in the Sac2 gene (23) might affect the expression of Bag3, a protein reported to impact synuclein clearance (27). However, brain levels of Bag3 were normal in the Sac2KO mice used for this study (*SI Appendix*, Fig. S1*B*).

The striking synthetic effect of the lack of Sac2 with the inactivating mutation in the Sac domain of SJ1 raise the possibility that that Sac2 may have some overlapping function with SJ1. Therefore, it was of interest to determine whether a pool of Sac2 is present in axon terminals and is associated with endocytic structures. Available anti-Sac2 antibodies did not reveal a reliable immunoreactivity in either brain tissue or neuronal cultures despite the reported enrichment of Sac2 in brain (22). Thus, we expressed GFP-Sac2 in WT cultured hippocampal neurons using either a lentivirus vector or a calcium-phosphate transfection. GFP-Sac2 had a diffuse and broad distribution throughout neurons, including axon and axon terminals, which were visualized by anti-synaptophysin immunostaining (*SI Appendix*, Fig. S2) or mCherry-Rab3 overexpression (Fig. 2*A*). Furthermore, when GFP-Sac2, which displays properties of a Rab5 effector (21, 22), was coexpressed with mRFP-Rab5, a striking recruitment of GFP-Sac2 to mRFP-Rab5–positive structures was observed in axons (Fig. 2*B*). Most likely, the diffuse cytosolic localization in the absence of mRFP-Rab5 overexpression is due to saturation of endogenous Rab5. This cytosolic pool of GFP-Sac2 was not abolished by expression of mCherry-Rab3. These results suggest the plausibility of overlapping roles of Sac2 and SJ1 in nerve terminals.

Accumulation of Endocytic Factors in Axon Terminals of SJ^{RQ}KI Neurons Is Enhanced by the Absence of Sac2. We previously reported the occurrence of a very robust exaggerated accumulation of endocytic factors, including clathrin coat components and their endocytic accessory factors, such as amphiphysin and auxilin, in nerve terminals of SJ1^{RQ}KI neurons both in situ (in all of several brain regions examined) and in neuronal cultures (17). Most likely, this abnormal accumulation of endocytic factors at synapses reflects their impaired shedding from membranes due to the lack of PI4P dephosphorylation by the Sac domain of SJ1, with a resulting accumulation of PI4P.

We performed a similar analysis on neuronal cortical cultures of WT, Sac2KO, SJ1^{RQ}KI, and Sac2KO/SJ1^{RQ}KI mice. No such accumulation/clustering was observed in nerve terminals of Sac2KO neurons relative to controls (Fig. 3); however, in Sac2KO/SJ1^{RQ}KI neurons, accumulation of amphiphysin 2, clathrin light chain (CLC), auxilin, and SJ1 itself was strongly more pronounced than in SJ1^{RQ}KI neurons, corroborating evidence for a synthetic effect of the two mutations (Fig. 3). As in the case of SJ1^{RQ}KI neurons (17), the enhanced presynaptic accumulation of endocytic factors observed in double-mutant cultured cortical neurons was more pronounced at inhibitory than at excitatory presynaptic terminals, as detected by immunolabeling for vGAT and vGlut1, respectively (*SI Appendix*, Fig. S3).

Since previous studies of Sac2 had revealed that pools of this protein are localized on several endocytic compartments (21, 22), we also analyzed the distribution of EEA1 (early endosomal marker) and LAMP1 (lysosome marker) in cultured cortical neurons of WT, Sac2KO, SJ1^{RQ}KI, and Sac2KO/SJ1^{RQ}KI mice. However, no obvious difference for any of these markers was

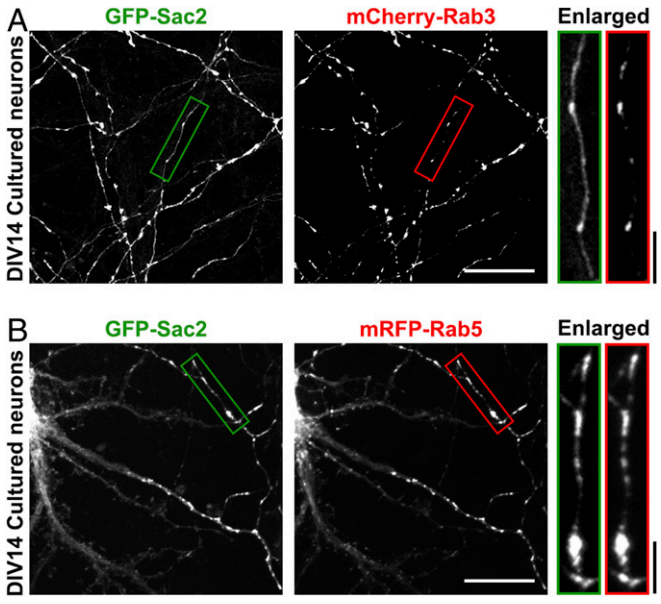

Fig. 2. GFP-Sac2 is present in axons and axon terminals. (*A* and *B*) Cultured WT hippocampal neurons were cotransfected with GFP-Sac2 and either mCherry-Rab3 (marker of axons) (*A*) or mRFP-Rab5 (*B*) at DIV8 and imaged at DIV14. The micrographs at the right show the areas bracketed by rectangles in the main fields at high magnification. In these enlargements, note the presence of a cytosolic axonal pool of Sac2 in mCherry-Rab3–expressing cells, while in cells expressing mRFP-Rab5, the cytosolic pool of GFP-Sac2 has relocalized to mRFP-Rab5–positive structures. (Scale bar: 20 μm; 5 μm for enlarged images.)

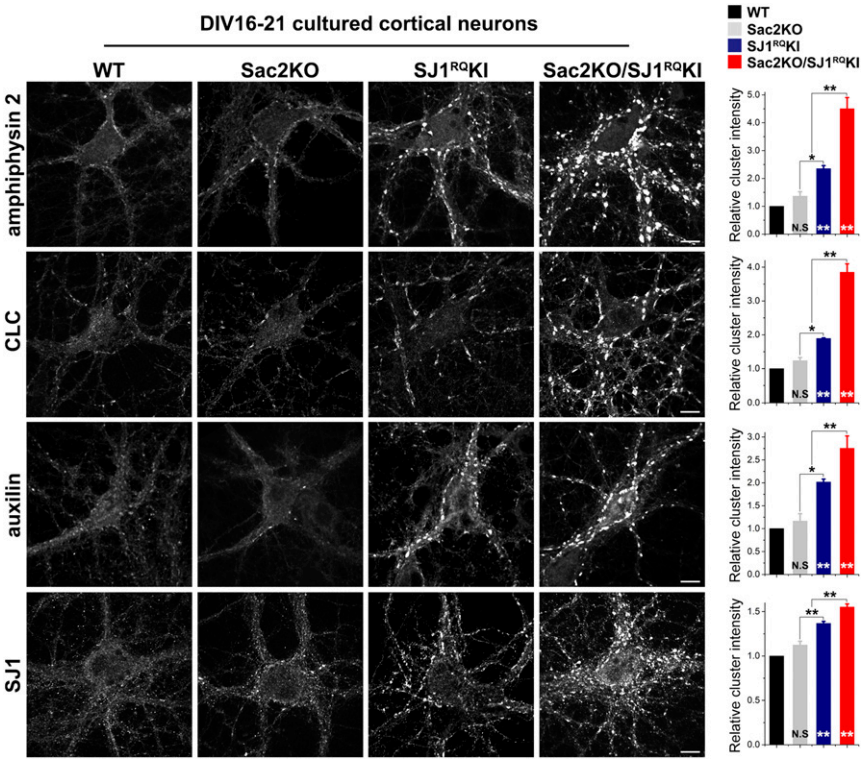

Fig. 3. The absence of Sac2 enhances the abnormal accumulation of endocytic factors observed at SJ1^{RQ}KI synapses. (*Left*) Representative images showing immunoreactivity for amphiphysin 2, CLC, auxilin, and SJ1 in DIV16 to 21 cultured cortical neurons from the genotypes indicated. (Scale bar: 10 μm.) (*Right*) Quantification of the synaptic clustering of each endocytic protein shown in the left panel. Amphiphysin 2: WT, $n = 39$; Sac2KO, $n = 43$; SJ1^{RQ}KI, $n = 38$; Sac2KO/SJ1^{RQ}KI, $n = 51$ (from five independent experiments). CLC: WT, $n = 36$; Sac2KO, $n = 34$; SJ1^{RQ}KI, $n = 32$; Sac2KO/SJ1^{RQ}KI, $n = 34$ (from three independent experiments). Auxilin: WT, $n = 27$; Sac2KO, $n = 20$; SJ1^{RQ}KI, $n = 29$; Sac2KO/SJ1^{RQ}KI, $n = 35$ (from three independent experiments). SJ1: WT, $n = 25$; Sac2KO, $n = 22$; SJ1^{RQ}KI, $n = 28$; Sac2KO/SJ1^{RQ}KI, $n = 24$ (from three independent experiments). Data are represented as mean ± SEM. N.S., not significant; $*P < 0.05$; $**P < 0.01$ by ANOVA and Tukey's post hoc test. Asterisks at the bottom of the bars represent the significance compared with control.

observed among the different genotypes, and clusters of amphiphysin 2 did not colocalize with these proteins (*SI Appendix*, Fig. S4).

Accumulation of Endocytic Factors in Axon Terminals Correlates with Accumulation of Abnormal Vesicular Intermediates. We next performed correlative light and electron microscopy (CLEM) to determine whether the clustered immunoreactivity of endocytic proteins corresponded to the accumulation of endocytic vesicular intermediates. Toward this aim, SNAP-tagged CLC was transfected into cultured cortical neurons grown on gridded glass coverslips and labeled with the cell-permeable Janelia Fluor 549. SNAP-CLC fluorescence colocalized with the prominent clusters of endogenous amphiphysin 2 (*SI Appendix*, Fig. S5*A*), indicating that this construct is targeted to presynaptic nerve terminals as the endogenous protein. SNAP-CLC–positive structures were then marked on the gridded glass coverslips, and selected regions were processed for epon embedding, thin sectioning and EM analysis (Fig. 4).

EM observation revealed that clusters of SNAP-CLC fluorescence in Sac2KO/SJ1^{RQ}KI double-mutant axon terminals corresponded to large varicose axon terminals as revealed by the massive presence of small vesicles and the presence of synaptic contacts (Fig. 4). However, these accumulations were clearly different from the clusters of bona fide synaptic vesicles of WT synapses (28) because of the larger spacing between them, which was occupied by a dense matrix (Fig. 4). In fact, when presynaptic active zones were visible in the section, a sharp boundary was observed between the typically tightly packed synaptic vesicles anchored to these zones (28) and the more loosely packed vesicles surrounding them (Fig. 4). At lower-power EM observation, these accumulations of loosely packed vesicles were reminiscent of the accumulation of clathrin-coated vesicles observed by EM around synaptic vesicle clusters at synapses of cultured neurons that either lack SJ1 (SJ1KO neurons) (2, 10) or lack all endophilins (endophilin triple KO neurons) (11), that is, the proteins that recruit SJ1 to endocytic sites (11, 29). However, in the case of Sac2KO/SJ1^{RQ}KI double-mutant cultured cortical neurons, clathrin coats could not be clearly observed on the loosely packed vesicles (Fig. 4) despite evidence of a high concentration of clathrin among them on immunofluorescence (Fig. 4). Most likely, these vesicles are partially uncoated vesicles, with clathrin and their accessory factors accounting for the matrix surrounding them. Dephosphorylation of PI(4,5)P_2 at the 5 position but with persistence of PI4P may be responsible for this phenotype.

The lack of an obvious assembled clathrin coat was also in contrast to what we had observed at synapses of SJ1^{RQ}KI adult brains in situ, where loosely spaced endocytic vesicular intermediates had a recognizable clathrin coat. However, when we examined nerve terminals of SJ1^{RQ}KI cortical neurons in culture, similarly loosely packed vesicles without a clear clathrin coat were observed (*SI Appendix*, Fig. S5*B*). While the reason for this discrepancy between EM observations at synapses in situ and in vitro remains to be elucidated, our current findings suggest that the absence of Sac2 simply results in an exaggeration of the trafficking defect of SJ1^{RQ}KI, not a qualitatively different defect.

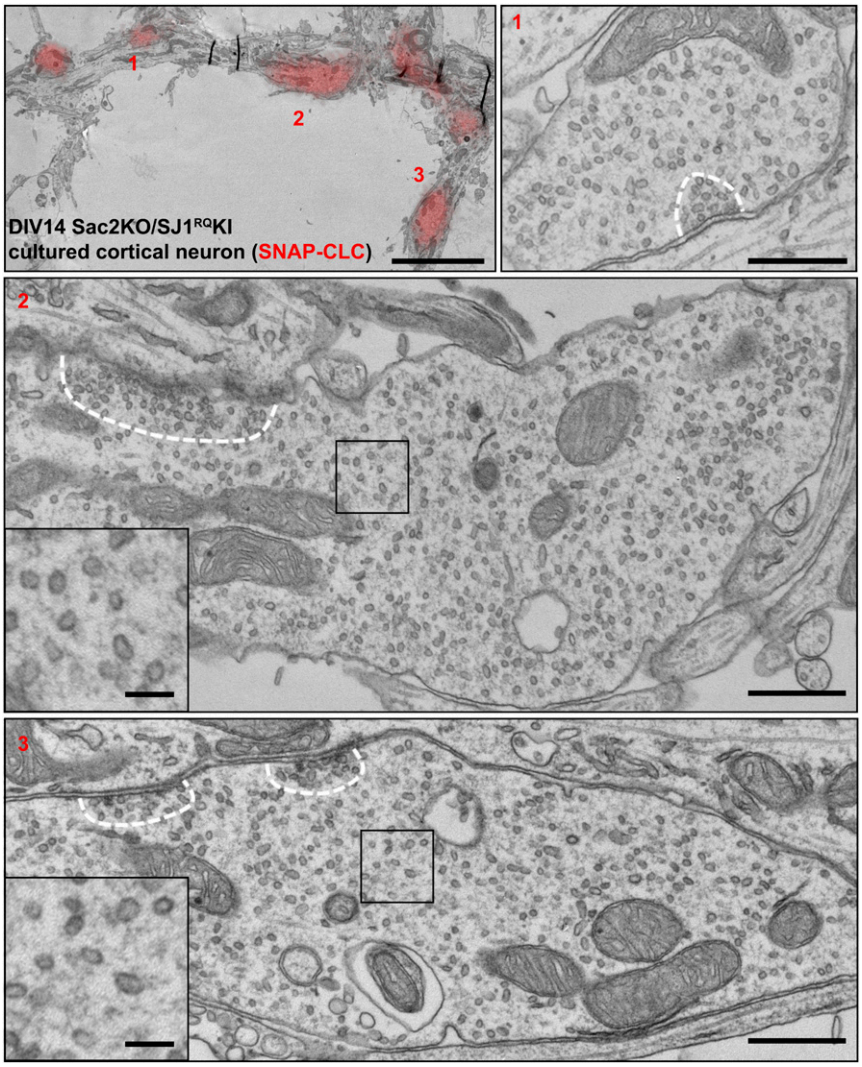

Fig. 4. Abnormal accumulation of small vesicles in Sac2KO/SJ1^{RQ}KI double-mutant presynaptic terminals. Cultured cortical neurons from Sac2KO/SJ1^{RQ}KI double-mutant mice were transfected with SNAP-CLC and incubated with Janelia Fluor 549 to perform CLEM. (*Top Left*) Low-magnification EM image aligned with the fluorescence image of SNAP-CLC (red). (Scale bar: 5 μm.) (*Top*, *Middle* and *Right* and *Bottom*) High-magnification EM images. Note the great abundance of loosely packed small vesicles surrounded by and intermixed with a dense protein matrix. The dashed white line outlines the sharp boundary of a classical cluster of tightly packed synaptic vesicles adjacent to a synaptic junction. These vesicles are in the same size range as the surrounding loosely packed vesicles. (Scale bars: 500 nm; 100 nm for the *Insets*.)

Lack of Sac2 Accelerates the Occurrence of Neurodegenerative Changes in SJ1^{RQ}KI Neurons. We previously showed that the level of the E3 ubiquitin ligase parkin, another PD gene (PARK2), is robustly increased in 6-mo-old SJ1^{RQ}KI mouse brains (17). We have now found that this increase is already observed at 3.5 mo but not at 2.5 mo (Fig. 5*A*). However, a Sac2KO/SJ1^{RQ}KI double-mutant mouse that survived for longer than 2 wk and was euthanized at 19 d showed a significant increase in parkin in the brain relative to brains of similar age from WT, SJ1^{RQ}KI, or Sac2KO mice (Fig. 5*B*), although no increase in parkin was observed in Sac2KO/SJ1^{RQ}KI double-mutant mouse brain at postnatal day (P) 0 (Fig. 5*C*). Moreover, lysates from 3-wk-old Sac2KO/SJ1^{RQ}KI double-mutant hippocampal neuronal cultures showed up-regulation of parkin relative to Sac2KO cultures and to WT and SJ1^{RQ}KI cultures of similar age (Fig. 5 *D* and *E*).

This earlier onset of a biochemical parameter that may reflect neurodegeneration was also reflected in an earlier occurrence of structural signs of neurodegeneration. In SJ1^{RQ}KI mice, age-dependent dystrophic changes were observed at 1 mo of age, but not at 2 wk, in a subset of axon terminals of nigrostriatal neurons, as revealed by immunofluorescence of frozen sections (17). These changes, which were revealed by abnormal clusters of immunoreactivity for markers of dopaminergic axons, such as tyrosine hydroxylase (TH) or the dopamine plasma membrane transporter (DAT), as well as of a general axonal marker (SNAP25), suggest a special vulnerability of dopaminergic neurons of the nigrostriatal pathway to the SJ1^{RQ} mutation (17). When the same analysis was performed on the rare Sac2KO/SJ1^{RQ}KI double-mutant mice that survived for 2 wk, similar TH- and DAT-positive sparse dystrophic axon terminals were detected in the dorsal striatum of two Sac2KO/SJ1^{RQ}KI mice at P15 and P19, indicating an earlier occurrence of axonal dystrophy, consistent with a synthetic effect of the absence of Sac2 and of Sac mutation of SJ1 (Fig. 5*F*).

Discussion

Our results reveal a striking synthetic effect in mice of loss-of-function mutations of two Sac phosphatase domain-containing proteins, SJ1 and Sac2. While mice with the PD-inactivating mutation in the Sac domain of SJ1 (SJ^{RQ}KI) have neurologic defects but

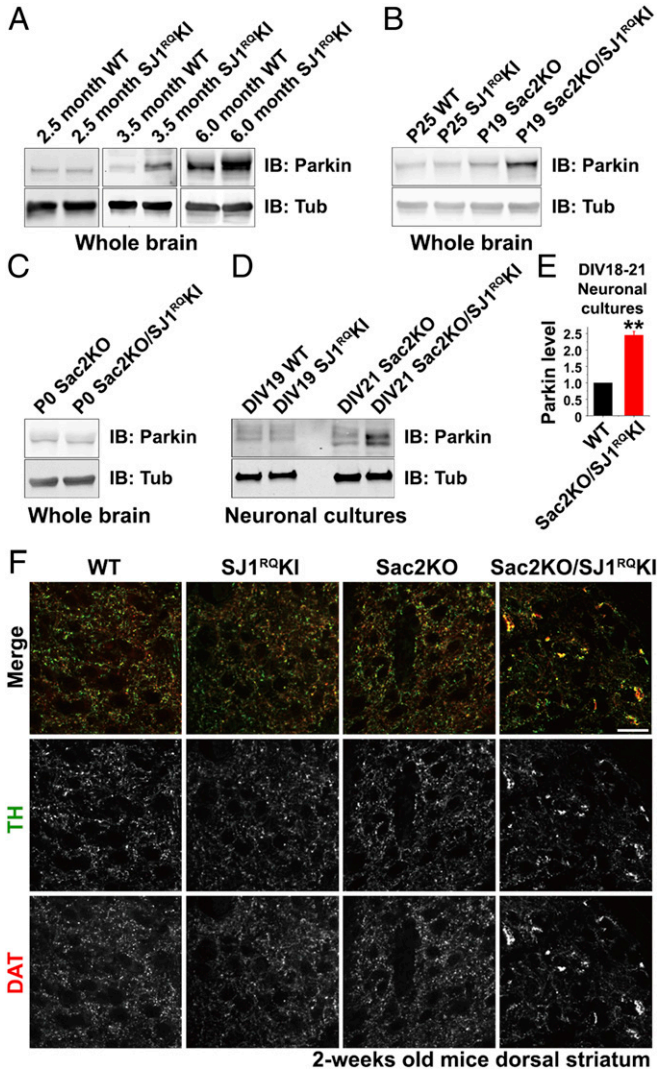

Fig. 5. The loss of Sac2 accelerates the occurrence of neurodegenerative phenotypes in SJ1^{RQ}KI neurons. (*A*) Levels of parkin in SJ1^{RQ}KI and a littermate WT control at three different ages as assessed by Western blot analysis. In this field and in the following fields anti-tubulin (Tub) antibodies served as loading controls. (*B*) Increase of parkin in a P19 Sac2KO/SJ1^{RQ}KI double-mutant brain relative to brains of a similar age from WT, SJ1^{RQ}KI, and Sac2KO mice. (*C*) Parkin level was unchanged in P0 Sac2KO/SJ1^{RQ}KI brain relative to its littermate control (Sac2KO). (*D*) Representative Western blot showing the up-regulation of parkin in Sac2KO/SJ1^{RQ}KI hippocampal neuron cultures relative to Sac2KO and to WT and SJ1^{RQ}KI cultures of similar age. (*E*) Quantification of the parkin level in Sac2KO/SJ1^{RQ}KI hippocampal neuron cultures relative to WT cultures of similar age (DIV18 to 21). $n = 3$ (from two independent neuronal cultures). Data are represented as mean ± SEM. N.S., not significant; $^{**}P < 0.01$, by Student's *t* test. (*F*) Anti-TH (green) and anti-DAT (red) immunofluorescence on frozen sections of dorsal striata of 2-wk-old mice of the indicated genotypes. Aggregation (coaggregation) of TH and DAT was observed only in Sac2KO/SJ1^{RQ}KI double-mutant striatum at this age. (Scale bar: 20 μm.)

generally survive to adulthood and Sac2KO mice do not have an obvious phenotype, the majority of mice with both mutations have severe neurologic defects and die perinatally, with none surviving to adulthood. A synthetic effect is also observed at the cellular level, as the absence of Sac2 enhances the presynaptic defects observed in SJ^{RQ}KI nerve terminals and anticipates the age at which parkin abnormally accumulates and dystrophic dopaminergic axons appear in the dorsal striatum. These results suggest that the Sac phosphatase domains of the two proteins have at least partially overlapping functions.

Sac2 is an inositol phosphatase preferentially expressed in the brain (22). It has been shown to associate with vesicular structures, including Rab5-positive endosomes in nonneuronal cells (21, 22), and also in proximity of Rab3-positive organelles in pancreatic β cells (30), but little is known about its localization in neurons, although a role in axons has been proposed (25). The synergistic effects of the absence of Sac2 on the presynaptic defects produced by the Sac R258Q mutation of SJ1, a protein enriched in nerve terminals, strongly suggest that at least some actions of Sac2 occur at the presynapse. Accordingly, although we could not assess the localization of the endogenous protein, we found that exogenous tagged Sac2 is present in axons and axon terminals and is recruited to Rab5-positive endosomes.

Nerve terminals of both SJ1^{RQ}KI and Sac2KO/SJ1^{RQ}KI neuronal cultures are characterized by a strikingly exaggerated accumulation of clathrin coat components and accessory factors, as well as by small vesicles in the size range of synaptic vesicles that surround, but are well separated from, the characteristic clusters of synaptic vesicles (28) anchored at presynaptic active zones. These other vesicles are not as tightly packed as typical synaptic vesicle clusters and are separated from one another by a dense matrix. The endocytic factors that accumulate in mutant nerve terminals are likely to be part of the matrix, as strongly suggested by the overlap between CLC fluorescence and these areas revealed by CLEM. Interconversion of phosphoinositide species on synaptic vesicle membranes by phosphorylation-dephosphorylation during their exo-endocytic cycle impacts their traffic by controlling the association-dissociation of cytosolic factors (31). Thus, these vesicles may represent endocytic intermediates that fail to progress to downstream stations due to the abnormal accumulation of an inappropriate phosphoinositide on their membrane.

The Sac domain of the synaptojanin family can dephosphorylate PI4P, PI3P, and PI(3,5)P_2 in vitro (32), although a main function of this Sac domain in living cells is thought to be the dephosphorylation of PI4P resulting from the action of its 5-phosphatase domain on PI(4,5)P_2 (31). The Sac domain of Sac2 acts nearly exclusively of PI4P (21, 22). Thus, we favor a model in which the combined absence of the two Sac phosphatase activities results in ectopic PI4P accumulation on synaptic membranes. This accumulation in turn may prevent complete shedding of endocytic factors whose binding to the membranes is primarily PI(4,5)P_2-dependent but may also depend in part on PI4P. We note that auxilin, the cochaperone of HSC70 needed for the disassembly of the clathrin cage after the release of clathrin adaptors, contains an N-terminal PTEN-homology module that binds phospholipids, including PI4P (33). Auxilin is one of the factors abnormally accumulated at SJ^{RQ}KI and Sac2KO/SJ1^{RQ}KI mutant synapses and may be responsible for the partial uncoating.

Defective endocytic flux along the endocytic pathway due to impaired shedding of endocytic factors may affect the reliability of synaptic transmission by resulting in a lower pool of reserve synaptic vesicles, as has been observed for mutations in several endocytic factors (11, 34–37). The occurrence of epileptic seizures in mice with these mutations reflects the greater dependence of inhibitory synapses on synaptic vesicle recycling given their high levels of tonic activity (38). Accordingly, even in our present study of primary cortical neuronal cultures, which comprise primarily inhibitory GABAergic interneurons and glutamatergic pyramidal neurons, inhibitory synapses were the most severely affected in Sac2KO/SJ1^{RQ}KI cultures.

It is also possible that defect in Sac phosphatase activity at synapses may have effects beyond synaptic vesicle recycling. A selective defect in the Sac domain of SJ1 in zebrafish and flies, including the KI of the R258Q mutation in flies, has been

reported to impact autophagy (39, 40), a process known to also occur in nerve terminals (41, 42), including nerve terminals of dopaminergic neurons (43, 44). It was proposed that such a defect could be explained by abnormal accumulation in nerve terminals of PI3P, a phosphoinositide required for the initial nucleation of the autophagy machinery (45). Recent work suggests that PI4P may also be needed at initial stages of autophagy (46). Another possibility is that abnormal endocytic traffic may affect the availability of ATG9, the transmembrane component of the core autophagy machinery (47, 48). The precise role of the Sac domain in autophagy merits further investigation.

Irrespective of the precise mechanisms through which the combined deficiency of Sac2 and of the Sac domain of SJ1 impact presynaptic function, our results have interesting implications for the PD field. The SJ1 R258Q mutation is responsible for familial (although rare) cases of PD (5–7), and Sac2 is located within a PD risk locus identified by genome-wide association studies (23). Our results provide evidence supporting the hypothesis that the gene encoding Sac2 is the PD risk gene and points to a shared site of action of the two proteins as a node whose dysfunction may result in PD pathogenesis. Other evidence links SJ1 function to PD. For example, endophilin, which has a major role in recruiting SJ1 to endocytic sites (11, 29), binds parkin (20), and loss of endophilin results in elevated levels of parkin (18, 20). Indeed, both endophilin and SJ1 are ubiquitinated by parkin (18, 20), and the endophilin A1 gene itself has been identified as a risk locus for PD (49). In addition, parkin is very robustly increased in $SJ1^{RQ}KI$ mouse brains (17), and here we found that the additional loss of Sac2 accelerates the occurrence of this phenotype. Finally, the PD protein LRRK2 (PARK8) phosphorylates SJ1, endophilin, and auxilin (50–52). Further elucidating how mutations of these housekeeping proteins impact neuronal functions and, more robustly, the function of selective PD-relevant neuronal populations is expected to advance our understanding of PD mechanisms.

Materials and Methods

Animals. $SJ1^{RQ}KI$ mice carrying the EOP R258Q mutation were custom-generated as reported previously (17). Sac2/INPPF5 KO mice were a gift from Dr. Jonathan Epstein, University of Pennsylvania (26). No obvious neurologic defects were observed in the Sac2KO mice. Both strains were maintained on the C57BL6/129 genetic background and crossed with each other to generate SJ1/Sac2 double-mutant mice. For the comparison of the four genotypes—WT, $SJ1^{RQ}KI$, Sac2KO, and $SJ1^{RQ}KI$/Sac2KO—SJ1 heterozygous KI (+/KI) mice were mated to generate homozygous mice (KI/KI) and WT littermate controls. Sac2KO/SJ1 heterozygous KI (+/KI) double-mutant mice were mated with each other to generate Sac2KO/$SJ1^{RQ}KI$ double-homozygous and Sac2 single-KO littermate controls. All mice were maintained on a 12-h light/dark cycle with standard mouse chow and water ad libitum. All research and animal care procedures were approved by the Yale University Institutional Animal Care and Use Committee.

Plasmids and Antibodies. The sources of cDNAs were as follows: pEGFPC-Sac2 and pSNAP-human CLC were generated in our laboratory, and pFUGW-GFP-Sac2 was generated from pEGFPC-Sac2 by Janelia Research Campus/HHMI. The following primary antibodies used in this study were generated in our laboratory: rabbit anti-SJ1 and rabbit anti-auxilin. Antibodies obtained from commercial sources were as follows: mouse anti-EEA1 from BD Biosciences; mouse anti-amphiphysin 2, rabbit anti-CLC, guinea pig anti-vGluT1 (AB5905), rabbit anti-TH (AB152), and rat anti-DAT (MAB369) from Millipore Sigma; rabbit anti-synaptophysin (101 002) and rabbit anti-vGAT (131 002) from Synaptic Systems; rat anti-LAMP1 (ID4) from Developmental Studies Hybridoma Bank; rabbit anti-BAG3 (10599-1-AP) from Proteintech, mouse anti-tubulin (T5168) from Millipore Sigma; rabbit anti-tubulin (PA1-21153) from Invitrogen; mouse anti-parkin (4211) from Cell Signaling Technology; and Alexa Fluor 488-, 594- and 647-conjugated secondary antibodies from Invitrogen. The rabbit anti-Sac2 antibody was a kind gift from Yuxin Mao, Cornell University.

Immunoblotting. Postnuclear supernatant of brain tissue was obtained by homogenization of mouse brain in buffer containing 20 mM Tris pH 7.4, 150 mM NaCl, and 2 mM ethylenediaminetetraacetic acid supplemented with protease inhibitors (cOmplete Protease Inhibitor Mixture; Roche) and subsequent centrifugation at 700 × *g* for 10 min. Protein concentration was determined using the Pierce BCA Protein Assay Kit. Sodium dodecyl sulfate polyacrylamide gel electrophoresis and Western blot analyses were performed following standard procedures. Proteins were detected by an enhanced chemiluminescence reagent and quantified by densitometry using Fiji software.

Primary Neuronal Culture and Fluorescence Microscopy. Cultures of cortical or hippocampal neurons were prepared from P0 to P2 neonatal mouse brains as described previously (35, 53) and used at days in vitro (DIV) 14 to 23. For lentivirus infection, DIV3 neurons cultured on 12-mm coverslips were infected with 1 μL of FUGW-GFP-Sac2 viruses (5E9 IU/mL) and fixed after DIV16. Calcium phosphate transfection was performed as described previously (53). Cells were fixed with 4% formaldehyde (freshly prepared from paraformaldehyde) in 0.1 M sodium phosphate pH 7.2 and 4% sucrose, blocked, and permeabilized with PBS containing 5% BSA and 0.1% Triton X-100. Primary and secondary antibody incubations for immunofluorescence were subsequently performed in the same buffer. After washing, samples were mounted on slides with Prolong Gold antifade reagent (Invitrogen) and observed using either a PerkinElmer Ultraview spinning disk confocal microscope equipped with a 60× CFI PlanApo VC objective or a Zeiss LSM 710 laser-scanning confocal microscope equipped with a 63× PlanApo objective.

CLEM. Plasmids encoding SNAP-CLC were electroporated into dissected neuronal suspensions using an Amaxa Nucleofector Kit (Lonza) at DIV0 before plating on 35-mm gridded, glass-bottom MatTek dishes (part no. P35G-1.5-14-CGRD). At DIV14, neurons were stained with 0.5 μM Janelia Fluor 549 at 37 °C for 1 h, followed by incubation in original culture medium at 37 °C for 2 h before fixation for immunofluorescence or CLEM. Labeled neurons were imaged and their coordinates on the MatTek dishes recorded using fluorescence microscopy and bright-field differential interference contrast microscopy, respectively. Then neurons were fixed with 2.5% glutaraldehyde in 0.1 M sodium cacodylate buffer, postfixed in 0.1 M sodium cacodylate buffer containing 1% OsO_4 and 1.5% $K_4Fe(CN)_6$ (Sigma-Aldrich), en bloc stained with 2% aqueous uranyl acetate, dehydrated, and embedded in Embed 812. The nerve terminals expressing SNAP-CLC were relocated (based on the prerecorded coordinates), sectioned, and imaged. Ultrathin sections (60 to 80 nm) were observed with a Philips CM10 microscope at 80 kV, and images were obtained with the iTEM soft imaging system and a Morada 1k × 1k CCD camera (Olympus). Except when noted otherwise, all reagents for EM were obtained from EMS.

Brain Histology. Brain tissues from 2-wk-old mice were dissected out, immersed immediately in ice-cold fixative (4% formaldehyde in 0.1 M phosphate buffer) and kept in the same fixative overnight at 4 °C. Brains were then transferred to increasing concentrations of sucrose (10%, 20% and 30% wt/vol) in PBS, embedded in Tissue-Tek OCT compound, and frozen in liquid nitrogen-cooled isopentane. Coronal or sagittal (15 to 30 μm thick) sections were cut with a cryostat and mounted on Superfrost Ultra Plus Adhesion slides (Thermo Fisher Scientific). Sections were then blocked and permeabilized with a solution containing 3% normal goat serum, 1% BSA, PBS, and 0.1% Triton-X100 for 1 h at room temperature; incubated with primary antibodies (diluted in the same buffer) overnight at 4 °C; washed; incubated with Alexa Fluor-conjugated secondary antibodies for 1 h at room temperature; and finally mounted with Prolong Gold antifade reagent with DAPI and sealed with nail polish. Images were acquired with a PerkinElmer Ultraview spinning disk confocal microscope equipped with a 40× objective.

Quantification of Immunoreactivity Clustering. Quantification of endocytic protein clustering was performed using Fiji software as follows. After background subtraction, the same threshold intensity was applied to all images, and raw intensity values of masked regions were measured using the "analyze particles" function of Fiji. Quantification of the average fluorescence of puncta larger than 0.1 μm^2 was performed for WT control, $SJ1^{RQ}KI$, Sac2KO, and Sac2KO/$SJ1^{RQ}KI$ neurons.

Statistical Analysis. Unless specified otherwise, data are presented as mean ± SEM. Statistical significance was determined using the Student's two-sample *t* test for the comparison of two independent groups or ANOVA followed by Tukey's honest significant difference post hoc test for multiple group comparisons. In the figures, $*P < 0.05$; $**P < 0.01$.

Data Availability. All relevant data are included in the main text and *SI Appendix*.

ACKNOWLEDGMENTS. We thank Frank Wilson and Rosemary Coolon for outstanding technical assistance, Dr. Jonathan Epstein (University of Pennsylvania) for the gift of Sac2KO mice, Yuxin Mao for the gift of anti-Sac2 antibodies, and Kimberley Ritola (HHMI Janelia Research Campus) for the generation of lentiviruses. This work was supported by grants from the NIH (NS36251 and DA018343), the Kavli Foundation, the Michael J. Fox Foundation, and the Parkinson's Foundation (to P.D.C.).

1. P. S. McPherson *et al*., A presynaptic inositol-5-phosphatase. *Nature* **379**, 353–357 (1996).
2. O. Cremona *et al*., Essential role of phosphoinositide metabolism in synaptic vesicle recycling. *Cell* **99**, 179–188 (1999).
3. D. A. Dyment *et al*., Homozygous nonsense mutation in SYNJ1 associated with intractable epilepsy and tau pathology. *Neurobiol. Aging* **36**, 1222 e1221-1225 (2015).
4. K. Hardies *et al*.; AR working group of the EuroEPINOMICS RES Consortium, Loss of SYNJ1 dual phosphatase activity leads to early-onset refractory seizures and progressive neurological decline. *Brain* **139**, 2420–2430 (2016).
5. C. E. Krebs *et al*., The Sac1 domain of SYNJ1 identified mutated in a family with early-onset progressive Parkinsonism with generalized seizures. *Hum. Mutat.* **34**, 1200–1207 (2013).
6. M. Quadri *et al*.; International Parkinsonism Genetics Network, Mutation in the SYNJ1 gene associated with autosomal recessive, early-onset Parkinsonism. *Hum. Mutat.* **34**, 1208–1215 (2013).
7. S. Olgiati *et al*., PARK20 caused by SYNJ1 homozygous Arg258Gln mutation in a new Italian family. *Neurogenetics* **15**, 183–188 (2014).
8. K. R. Schuske *et al*., Endophilin is required for synaptic vesicle endocytosis by localizing synaptojanin. *Neuron* **40**, 749–762 (2003).
9. P. Verstreken *et al*., Synaptojanin is recruited by endophilin to promote synaptic vesicle uncoating. *Neuron* **40**, 733–748 (2003).
10. M. Hayashi *et al*., Cell- and stimulus-dependent heterogeneity of synaptic vesicle endocytic recycling mechanisms revealed by studies of dynamin 1-null neurons. *Proc. Natl. Acad. Sci. U.S.A.* **105**, 2175–2180 (2008).
11. I. Milosevic *et al*., Recruitment of endophilin to clathrin-coated pit necks is required for efficient vesicle uncoating after fission. *Neuron* **72**, 587–601 (2011).
12. A. Fotin *et al*., Structure of an auxilin-bound clathrin coat and its implications for the mechanism of uncoating. *Nature* **432**, 649–653 (2004).
13. E. Eisenberg, L. E. Greene, Multiple roles of auxilin and hsc70 in clathrin-mediated endocytosis. *Traffic* **8**, 640–646 (2007).
14. S. Edvardson *et al*., A deleterious mutation in DNAJC6 encoding the neuronal-specific clathrin-uncoating co-chaperone auxilin, is associated with juvenile parkinsonism. *PLoS One* **7**, e36458 (2012).
15. Ç. Köroğlu, L. Baysal, M. Cetinkaya, H. Karasoy, A. Tolun, DNAJC6 is responsible for juvenile parkinsonism with phenotypic variability. *Parkinsonism Relat. Disord.* **19**, 320–324 (2013).
16. S. Olgiati *et al*., DNAJC6 mutations associated with early-onset Parkinson's disease. *Ann. Neurol.* **79**, 244–256 (2015).
17. M. Cao *et al*., Parkinson Sac domain mutation in synaptojanin 1 impairs clathrin uncoating at synapses and triggers dystrophic changes in dopaminergic axons. *Neuron* **93**, 882–896 e5 (2017).
18. M. Cao, I. Milosevic, S. Giovedi, P. De Camilli, Upregulation of Parkin in endophilin mutant mice. *J. Neurosci.* **34**, 16544–16549 (2014).
19. S. Matta *et al*., LRRK2 controls an EndoA phosphorylation cycle in synaptic endocytosis. *Neuron* **75**, 1008–1021 (2012).
20. J. F. Trempe *et al*., SH3 domains from a subset of BAR proteins define a Ubl-binding domain and implicate parkin in synaptic ubiquitination. *Mol. Cell* **36**, 1034–1047 (2009).
21. F. Nakatsu *et al*., Sac2/INPP5F is an inositol 4-phosphatase that functions in the endocytic pathway. *J. Cell Biol.* **209**, 85–95 (2015).
22. F. Hsu, F. Hu, Y. Mao, Spatiotemporal control of phosphatidylinositol 4-phosphate by Sac2 regulates endocytic recycling. *J. Cell Biol.* **209**, 97–110 (2015).
23. M. A. Nalls *et al*.; International Parkinson's Disease Genomics Consortium (IPDGC); Parkinson's Study Group (PSG) Parkinson's Research: The Organized GENetics Initiative (PROGENI); 23andMe; GenePD; NeuroGenetics Research Consortium (NGRC); Hussman Institute of Human Genomics (HIHG); Ashkenazi Jewish Dataset Investigator; Cohorts for Health and Aging Research in Genetic Epidemiology (CHARGE); North American Brain Expression Consortium (NABEC); United Kingdom Brain Expression Consortium (UKBEC); Greek Parkinson's Disease Consortium; Alzheimer Genetic Analysis Group, Large-scale meta-analysis of genome-wide association data identifies six new risk loci for Parkinson's disease. *Nat. Genet.* **46**, 989–993 (2014).
24. C. Blauwendraat *et al*.; 23andMe Research Team; International Parkinson's Disease Genomics Consortium (IPDGC), Parkinson's disease age at onset genome-wide association study: Defining heritability, genetic loci, and α-synuclein mechanisms. *Mov. Disord.* **34**, 866–875 (2019).
25. Y. Zou *et al*., Gene-silencing screen for mammalian axon regeneration identifies Inpp5f (Sac2) as an endogenous suppressor of repair after spinal cord injury. *J. Neurosci.* **35**, 10429–10439 (2015).
26. W. Zhu *et al*., Inpp5f is a polyphosphoinositide phosphatase that regulates cardiac hypertrophic responsiveness. *Circ. Res.* **105**, 1240–1247 (2009).
27. Y. L. Cao *et al*., A role of BAG3 in regulating SNCA/α-synuclein clearance via selective macroautophagy. *Neurobiol. Aging* **60**, 104–115 (2017).
28. D. Milovanovic, Y. Wu, X. Bian, P. De Camilli, A liquid phase of synapsin and lipid vesicles. *Science* **361**, 604–607 (2018).
29. H. Gad *et al*., Fission and uncoating of synaptic clathrin-coated vesicles are perturbed by disruption of interactions with the SH3 domain of endophilin. *Neuron* **27**, 301–312 (2000).
30. P. M. Nguyen *et al*., The PI(4)P phosphatase Sac2 controls insulin granule docking and release. *J. Cell Biol.* **218**, 3714–3729 (2019).
31. O. Cremona, P. De Camilli, Phosphoinositides in membrane traffic at the synapse. *J. Cell Sci.* **114**, 1041–1052 (2001).
32. S. Guo, L. E. Stolz, S. M. Lemrow, J. D. York, SAC1-like domains of yeast SAC1, INP52, and INP53 and of human synaptojanin encode polyphosphoinositide phosphatases. *J. Biol. Chem.* **274**, 12990–12995 (1999).
33. R. Guan, H. Dai, S. C. Harrison, T. Kirchhausen, Structure of the PTEN-like region of auxilin, a detector of clathrin-coated vesicle budding. *Structure* **18**, 1191–1198 (2010).
34. A. Luthi *et al*., Synaptojanin 1 contributes to maintaining the stability of GABAergic transmission in primary cultures of cortical neurons. *J. Neurosci.* **21**, 9101–9111 (2001).
35. S. M. Ferguson *et al*., A selective activity-dependent requirement for dynamin 1 in synaptic vesicle endocytosis. *Science* **316**, 570–574 (2007).
36. B. Zhang *et al*., Synaptic vesicle size and number are regulated by a clathrin adaptor protein required for endocytosis. *Neuron* **21**, 1465–1475 (1998).
37. T. W. Koh, P. Verstreken, H. J. Bellen, Dap160/intersectin acts as a stabilizing scaffold required for synaptic development and vesicle endocytosis. *Neuron* **43**, 193–205 (2004).
38. E. Evergren, E. Zotova, L. Brodin, O. Shupliakov, Differential efficiency of the endocytic machinery in tonic and phasic synapses. *Neuroscience* **141**, 123–131 (2006).
39. A. A. George, S. Hayden, G. R. Stanton, S. E. Brockerhoff, Arf6 and the 5′ phosphatase of synaptojanin 1 regulate autophagy in cone photoreceptors. *BioEssays* **38** (suppl 1), S119–S135 (2016).
40. R. Vanhauwaert *et al*., The SAC1 domain in synaptojanin is required for autophagosome maturation at presynaptic terminals. *EMBO J.* **36**, 1392–1411 (2017).
41. A. K. Stavoe, S. E. Hill, D. H. Hall, D. A. Colón-Ramos, KIF1A/UNC-104 transports ATG-9 to regulate neurodevelopment and autophagy at synapses. *Dev. Cell* **38**, 171–185 (2016).
42. A. K. H. Stavoe, E. L. F. Holzbaur, Autophagy in neurons. *Annu. Rev. Cell Dev. Biol.* **35**, 477–500 (2019).
43. D. Hernandez *et al*., Regulation of presynaptic neurotransmission by macroautophagy. *Neuron* **74**, 277–284 (2012).
44. L. G. Friedman *et al*., Disrupted autophagy leads to dopaminergic axon and dendrite degeneration and promotes presynaptic accumulation of α-synuclein and LRRK2 in the brain. *J. Neurosci.* **32**, 7585–7593 (2012).
45. M. Wirth, J. Joachim, S. A. Tooze, Autophagosome formation—The role of ULK1 and Beclin1-PI3KC3 complexes in setting the stage. *Semin. Cancer Biol.* **23**, 301–309 (2013).
46. D. Judith *et al*., ATG9A shapes the forming autophagosome through Arfaptin 2 and phosphatidylinositol 4-kinase IIIβ. *J. Cell Biol.* **218**, 1634–1652 (2019).
47. B. Ravikumar, K. Moreau, L. Jahreiss, C. Puri, D. C. Rubinsztein, Plasma membrane contributes to the formation of pre-autophagosomal structures. *Nat. Cell Biol.* **12**, 747–757 (2010).
48. J. L. Webber, A. R. Young, S. A. Tooze, Atg9 trafficking in mammalian cells. *Autophagy* **3**, 54–56 (2007).
49. D. Chang *et al*.; International Parkinson's Disease Genomics Consortium; 23andMe Research Team, A meta-analysis of genome-wide association studies identifies 17 new Parkinson's disease risk loci. *Nat. Genet.* **49**, 1511–1516 (2017).
50. P. Y. Pan *et al*., Parkinson's disease-associated LRRK2 hyperactive kinase mutant disrupts synaptic vesicle trafficking in ventral midbrain neurons. *J. Neurosci.* **37**, 11366–11376 (2017).
51. A. M. Arranz *et al*., LRRK2 functions in synaptic vesicle endocytosis through a kinase-dependent mechanism. *J. Cell Sci.* **128**, 541–552 (2015).
52. M. Nguyen, D. Krainc, LRRK2 phosphorylation of auxilin mediates synaptic defects in dopaminergic neurons from patients with Parkinson's disease. *Proc. Natl. Acad. Sci. U.S.A.* **115**, 5576–5581 (2018).
53. D. Park *et al*., Impairment of release site clearance within the active zone by reduced SCAMP5 expression causes short-term depression of synaptic release. *Cell Rep.* **22**, 3339–3350 (2018).